Engineering Geology 342 (2024) 107761

Contents lists available at ScienceDirect

Engineering Geology

journal homepage: www.elsevier.com/locate/enggeo

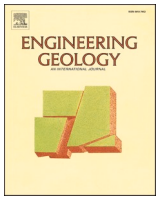

Four years of landslide observation with anthropogenic loading as an additional trigger - Analysis of seasonal and annual variability of physical parameters

Artur Marciniak [a,*], Sebastian Kowalczyk [b], Szymon Oryński [a], Justyna Cader [c], Jonathan Chambers [d], Iwona Stan-Kłeczek [e], Mariusz Majdański [a]

[a] Institute of Geophysics, Polish Academy of Sciences, 01-452 Warszawa, ul. Księcia Janusza 64, Poland
[b] Faculty of Geology, University of Warsaw, 02-089 Warszawa, ul. Żwirki i Wigury 93, Poland
[c] Mineral and Energy Economy Research Institute, Polish Academy of Sciences, 31-261 Kraków, ul. Wybickiego 7A, Poland
[d] British Geological Survey, Keyworth, Nottingham NG12 5GG, United Kingdom
[e] Faculty of Natural Sciences, University of Silesia, 41-200 Sosnowiec, ul. Będzińska 60, Poland

ARTICLE INFO

Keywords:
Landslides
MASW
Time-lapse measurements
Outer Carpathians
Anthropogenic
FDEM

ABSTRACT

Determining the structure and evolution of landslides is crucial for geophysical hazard assessment. In this study, we employed an approach integrating the methodologies of multi-channel analysis of surface waves (MASW) and electrical conductivity to image temporal and spatial changes within a landslide in southern Poland. The area, located in the Outer Carpathians, experiences significant climate fluctuations, compounded by anthropogenic activities such as recreational skiing requiring artificial snow.

Our combined seismic and electrical methods techniques reveal the landslide's susceptibility to environmental factors on both annual and seasonal scales. Additional analysis, including data clustering and remote sensing, identifies three distinct landslide zones with varying vulnerability to natural and anthropogenic influences.

While focusing on a specific area, our approach has global applicability to similar mass movements. This research addresses a gap in understanding time-dependent geophysical observations of moisture-driven landslides, providing valuable insights for hazard identification and mitigation strategies.

1. Introduction

Landslides, as geohazards, represent complex systems requiring comprehensive understanding and monitoring, especially considering their susceptibility to external influences (Arbanas and Arbanas, 2014; Uhlemann et al., 2017). This vulnerability encompasses both natural factors, including alterations in precipitation patterns (Villacorta et al., 2015), and anthropogenic impacts associated with land use change and development (Anbalagan et al., 2008).

A particular case highlighting anthropogenic factors is landsliding associated with ski slopes in mountainous environments, as considered in this study. Due to their unique characteristics, these slopes exhibit significant differences compared to their surrounding environments (de Jong et al., 2015). These changes are a result of terrain modifications, such as slope inclination, widening of trails, grading work, as well as the utilization of machinery such as grooming machines and snowmakers. Such factors impact not only the condition of the soil and snow cover but also hydrological and ecological processes within the slope. Understanding the interplay of these diverse factors and their implications for landslides is crucial, especially as part of efforts to mitigate natural hazards (United Nations, 2015).

The issue of studying landslides triggered by human involvement is particularly challenging. This problem has been widely examined in the context of densely populated areas (Knapen et al., 2006; Sabatakakis et al., 2005; Vranken et al., 2015). Growing numbers of studies are now addressing this geohazard within the framework of increasing urbanization in mountainous regions (Anbalagan et al., 2008; Ding et al., 2023; Keiler et al., 2023). Landslides are becoming more prevalent in

Abbreviation: FDEM, frequency domain electromagnetic method; EM, electromagnetic; MASW, multichannel analysis of surface waves; QC, quality control; RMS, root mean square; V_S, shear wave velocities.

* Corresponding author.
E-mail address: amarciniak@igf.edu.pl (A. Marciniak).

https://doi.org/10.1016/j.enggeo.2024.107761
Received 15 April 2024; Received in revised form 27 July 2024; Accepted 9 October 2024
Available online 10 October 2024

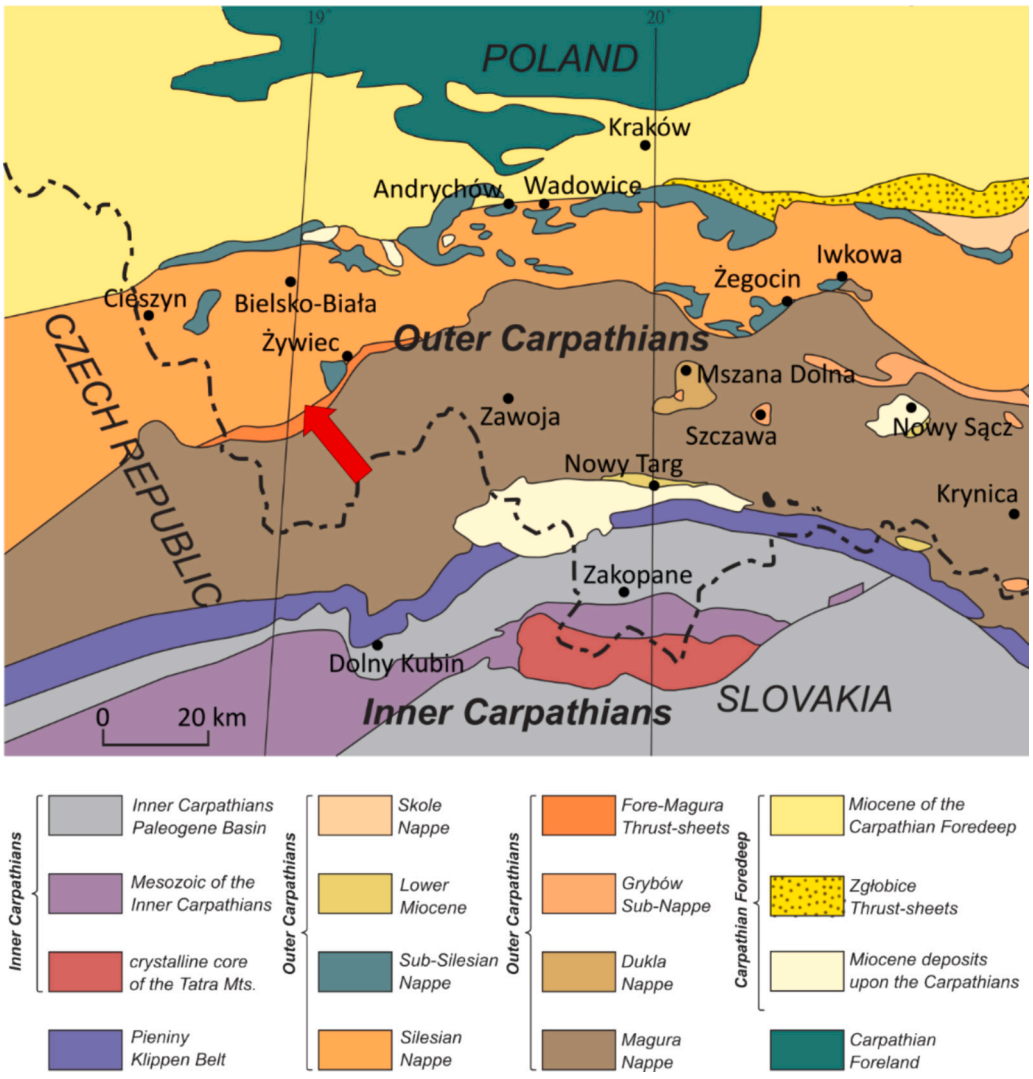

Fig. 1. Tectonic sketch map of the Polish Carpathians (according to Oszczypko et al., 2008, modified). The red arrow indicates the approximate location of the study. (For interpretation of the references to colour in this figure legend, the reader is referred to the web version of this article.)

mountainous areas worldwide, yet the complex geological terrain and the interplay of various influencing drivers hinder the availability of landslide-related data in these areas, thereby complicating accurate prediction and monitoring efforts (Aslan et al., 2020; Keiler et al., 2023; Li et al., 2023). Simultaneously, the need to recognize spatial patterns of landslide activity at the local scale is emphasized (Wistuba et al., 2024). In addressing these issues, resilient and cost-effective integrated systems deployable on vulnerable slopes prove helpful. Geophysical imaging significantly enhances these local landslide early warning systems, refining their design and monitoring with improved spatial and temporal resolutions (Whiteley et al., 2021a, 2021b).

Geophysical investigation of landslides has been an ongoing area of interest (Flores Orozco et al., 2018). Surface and seismological monitoring are the most commonly utilized methods (Amatya et al., 2021; Le Breton et al., 2021; Smail et al., 2022). Among geophysical imaging techniques, seismic tomography (Whiteley et al., 2020), electrical resistivity (Crawford et al., 2018; Jongmans et al., 2000; Kamiński et al., 2021; Lapenna et al., 2005), or their combinations (Godio et al., 2006; Hussain et al., 2020; Marciniak et al., 2021; Pazzi et al., 2019) are frequently employed. Particularly applicable to understanding shallow landslide conditions are methods such as multichannel analysis of surface waves (MASW) and frequency domain electromagnetic method (FDEM), which results show good consistency with landslide mass structure identified by other approaches (Furuya et al., 2013; Marciniak et al., 2021). MASW, despite increasing uncertainty in the results with depth (Wood and Cox, 2012), offers valuable insights into the horizontal and temporal variability of landslides, while the electromagnetic survey can provide complementary data, enhancing the overall understanding of the internal structure and allowing monitoring of changes in moisture content (Altdorff et al., 2018).

Recent trends indicate a shift towards adopting a multi-method approach (Bichler et al., 2004; Gallardo and Meju, 2004; Lu et al., 2024; Pistillo et al., 2024; Wróbel et al., 2023). Notably, studies holistically integrating the aforementioned techniques in a time-lapse scheme are relatively unexplored (Lapenna and Perrone, 2022; Lebourg et al., 2010; Wilkinson et al., 2010). Such integration necessitates a specialized approach to analysing the uncertainty of results obtained from each method (Hasan and Shang, 2022; Marciniak et al., 2019). This issue is increasingly recognized but remains relatively under-discussed in geophysics, particularly in the context of landslide zone imaging (Whiteley et al., 2021b).

The topic presented in this paper, determining changes in parameters in the near-surface zone, is considered relevant to the description of mass movement occurrences. The research presents findings from a 4-year investigation of a landslide located in the village of Cisiec, within the Żywiec district of the Silesian province, Poland. The study area is

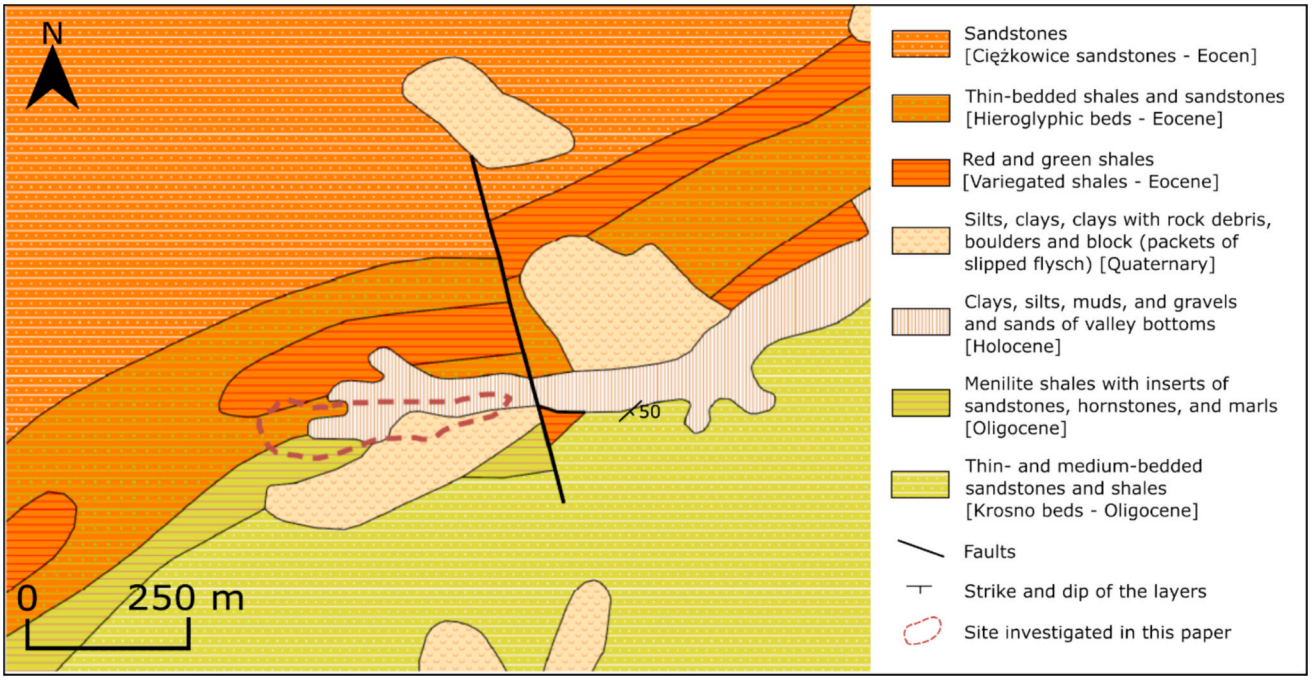

Fig. 2. Geological map of the study area (according to PGI-NRI, 2023, modified).

susceptible to both changing climatic conditions and human influence in the form of ski slope management, particularly snowmaking. This activity is aimed at counteracting the natural evolution of the environment, in which precipitation characteristics change towards longer rainfall, intense foehn winds and longer periods with positive temperatures. On the other hand, human activity leads to additional stress on the landslide-prone slope in the form of a large mass of heavy artificial snow, amplified effects in the form of freeze-thaw and subsequent hydrological changes including increased water saturation of the massif during the snowmelt period as a result of the differences between man-made and natural snow (Rixen et al., 2003). The combination of natural and dependent anthropogenic factors of varying seasonal intensity manifested in the form of the investigated landslide. The development of research methods for such landslide-prone areas is an urgent matter, specifically in the context of infrastructure construction in increasingly vulnerable terrains and expanding urbanization. From this perspective, the Cisiec study area can be treated as a full-scale landslide model, in which anthropogenic and natural factors are known, and their impact can be demonstrated using time-lapse geophysical monitoring. Geophysical techniques, including active seismic and electrical conductivity measurements, were employed. These were complemented by surface observations facilitated through laser scanning.

The susceptibility of the initial meters of the rock mass to environmental and anthropogenic factors ultimately controls the overall response of a landslide, regardless of the depth of its slip zone. In this instance, the zone within the first 15 m emerges as the most sensitive area, where numerous processes occur, including increased surface stresses and ground freezing during winter. Hence, it is imperative to enhance our understanding of the phenomena occurring in the context of geoengineering techniques employed for landslide stabilization, as well as in the domain of construction activities in analogous terrains.

The key novelty of this study lies in the integration of a time-lapse MASW survey with conductometry and remote sensing techniques applied to a landslide influenced by significant human factors. Our results demonstrate the potential for improving the interpretation of mass movement development through the utilization of a multi-method approach, observations over a several-year period and machine learning-assisted interpretation considering various parameters.

2. Study site

2.1. Geological context

The landslide examined in this study is located in southern Poland, specifically in the village of Cisiec near Węgierska Górka, within the Silesian Voivodeship. The study area lies in the Outer Western Carpathians (Fig. 1), within the Beskidy Mountains, and is part of the Silesian nappe, which is subdivided into the lower Cieszyn unit and the upper Godula unit (Paul et al., 1996).

The research site is characterized by the presence of Hieroglyphic beds and variegated shales. The Hieroglyphic beds consist of thin-bedded, fine-grained sandstones and grey, black, or dark green shales dating back to the Eocene. The thickness of the entire complex may reach up to 150 m (Golonka and Waśkowska-Oliwa, 2007).

The variegated shales formed under similar tranquil sedimentation conditions during the middle and late Eocene, and their thickness is approximately 70 m. These lithostratigraphic units overlap with each other. The Hieroglyphic beds lie on the Ciężkowice sandstones or variegated shales and beneath menilite shales. The Ciężkowice sandstones of the Eocene age are thick-bedded, fine-grained sandstones with irregular fractional layering (Ryłko, 2013). The variegated shale lies on top of the Istebna layers and underneath the Hieroglyphic or menilite beds. The thickness of the entire unit may reach up to 200 m (Golonka and Waśkowska-Oliwa, 2007). The youngest (Holocene) sediments in this area are colluvial clays, clays with rock debris, boulders and blocks (packets of flysch) and alluvial sediments in the river valley (Fig. 2). These complex geological conditions contribute to increased susceptibility to mass movements.

The active landslide is located on the northeastern slope. The site occupies a clearing surrounded by forest and spans the central part of the meadow. The direction of movement of the landslide is east-northeast, and the height difference is about 100 m. The slope of the concave type on which the landslide is located is inclined at an angle of 12 degrees. The area of the landslide is estimated at 3.77 ha (Kucharska and Kamiński, 2008). It is initially estimated to be about 456 m long and 130 m wide.

The bedrock of the landslide consists of the shale and sandstone

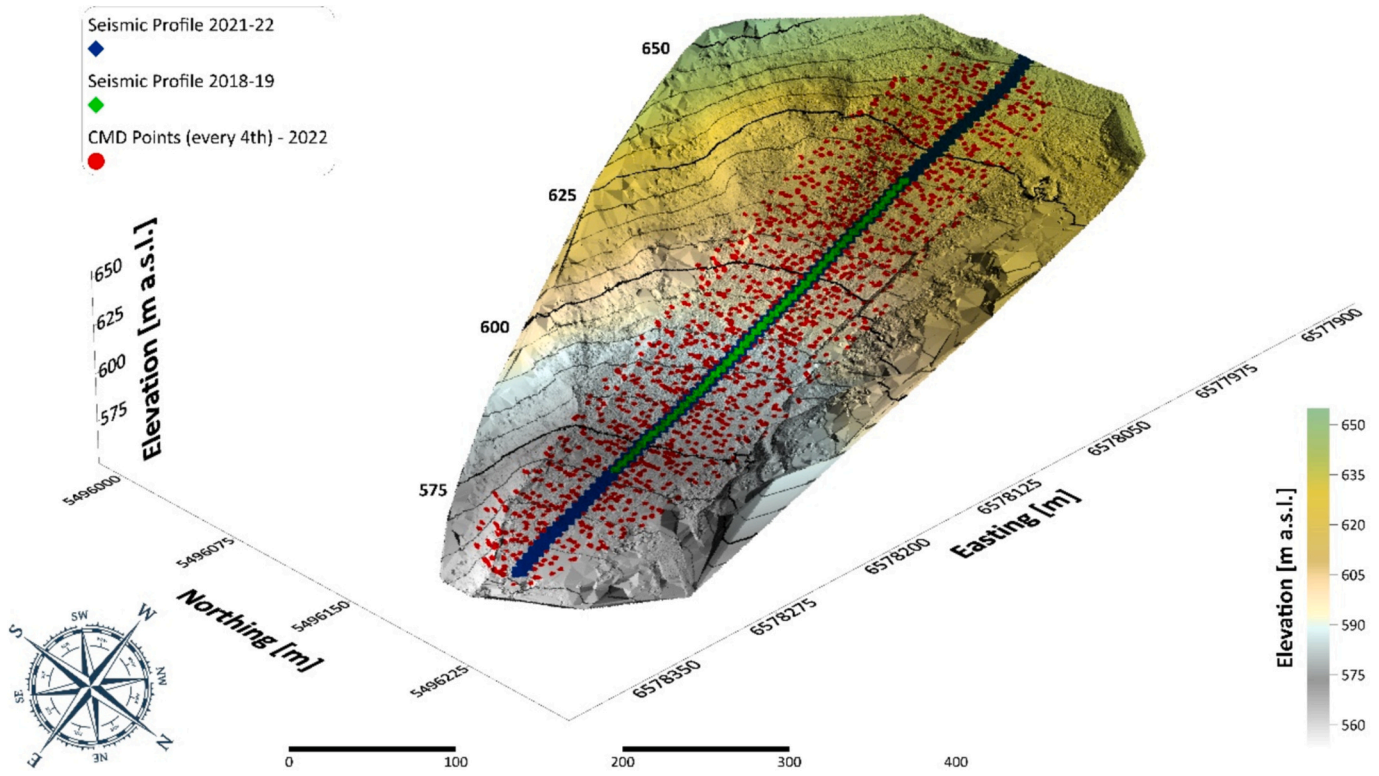

Fig. 3. The study site with located seismic lines across the sliding structure marked as green (2018, 2019) and blue (2021 and 2022) with FDEM profiles marked in red as CMD points. (For interpretation of the references to colour in this figure legend, the reader is referred to the web version of this article.)

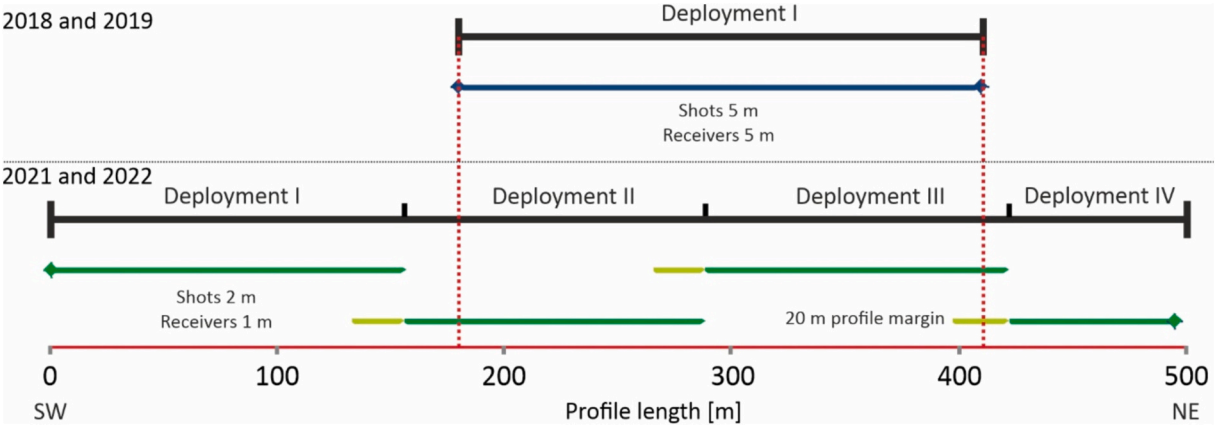

Fig. 4. The fieldwork scheme used for seismic data acquisition. Red dashed lines mark the common profile section for all four years. In 2021 and 2022, denser 1 m geophone spacing was deployed, with profile margins for the best possible data coverage. (For interpretation of the references to colour in this figure legend, the reader is referred to the web version of this article.)

described above, and the colluvial material consists of detrital-block components. The thickness of the landslide decreases in a northerly direction, with preliminary geophysical analysis (Marciniak et al., 2021) identifying the depth of the main slip surface in the range of 16 to 36 m (no borehole data available from this area). There are secondary scarps within the landslide. Additionally, watercourses along the northern and southern sides, as well as subsurface flows, are present along the slope.

Although the original trigger of landslide movement was described as being related to complex geology and rainwater infiltration (Kucharska and Kamiński, 2008), the construction of a ski lift on the Cisiec slope in 2011–2013 led to deforestation and extended snow cover, contributing to increased intensity of landslide movements.

2.2. Fieldwork

The fieldwork was conducted in October 2018, 2019, 2021, and June 2022 for the MASW survey, and October 2022 for electrical conductivity measurements (Fig. 3). The laser scanning data was collected in May 2019. Such a scheme allowed for the monitoring of yearly as well as seasonal changes in the subsurface with data for correlation of surface and subsurface observations.

During the first two years of observations, a shorter 230 m line was deployed for seismic investigations across the main part of the sliding body (Fig. 4). In later years, the observations were extended, with the use of denser 1 m geophone spacing for high-resolution data acquisition. During the years 2018–2022, the weather conditions remained similar, providing unbiased registration in terms of surface water flows caused

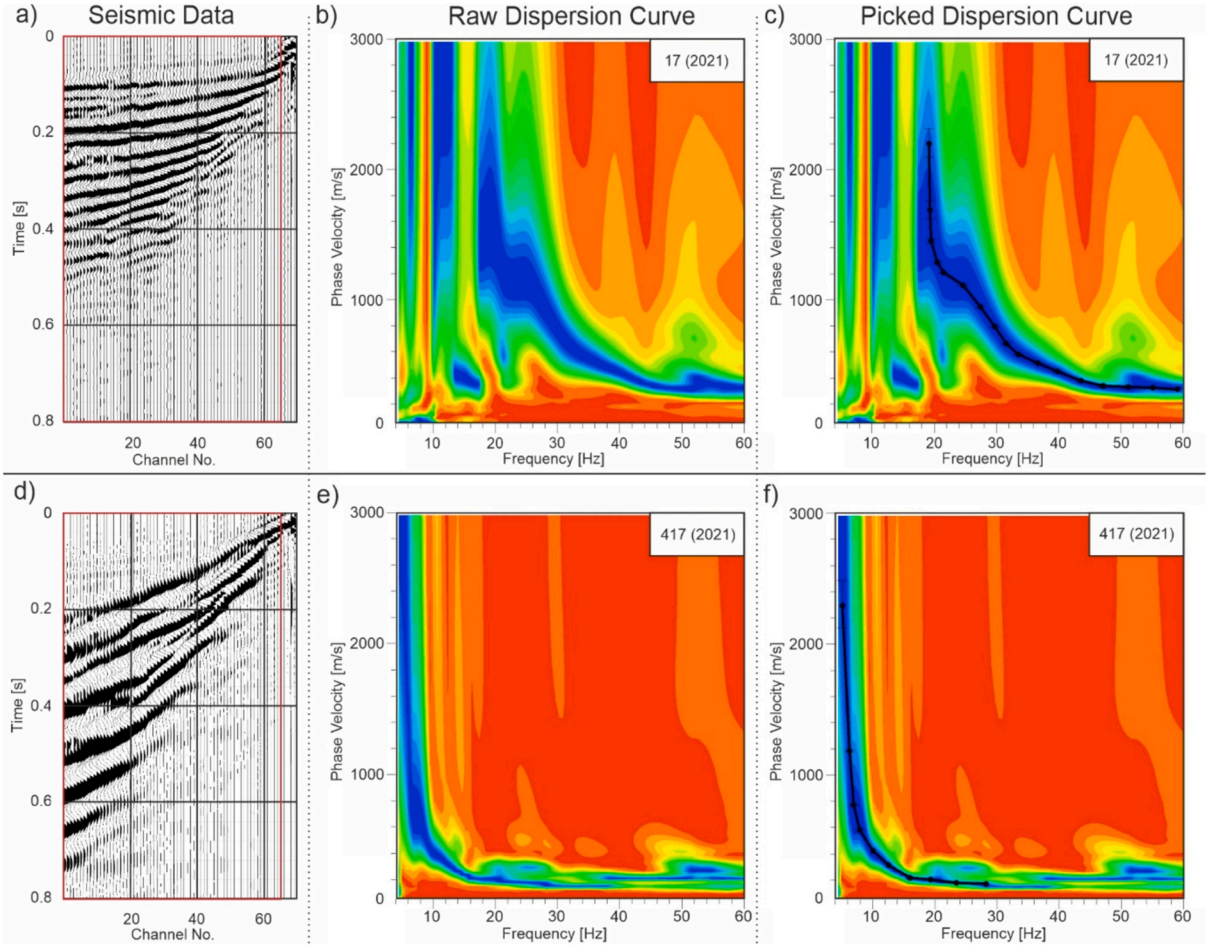

Fig. 5. Example of raw data (a, d) for positions 17 and 417 of 2021, with marked 60 m analysis window and 10 m offset from the shot point (red window). The dominance of lower-frequency Rayleigh waves can be seen in the data from position 417 m (d). Examples of the obtained dispersion curves reveal different characteristics for the upper and lower parts of the landslide (b, e). Data from each measurement point were picked three times and then averaged. This approach made it possible to estimate the uncertainty of the picking, which is low as presented by the visible error bars (e, f). (For interpretation of the references to colour in this figure legend, the reader is referred to the web version of this article.)

by rainfall. The data gathered in 2022 was recorded after the snowmelt period.

Similarly to previous data gatherings, the surface was dry, and no rainfall occurred during the fieldwork period. In all cases, an 8 kg sledgehammer with strikes into steel plate repeated three times for each shot point was used. The geophones used had a natural frequency of 4.5 Hz in all cases and were recording vertical component of ground motion. Acquisitions were made using ABEM Teraloc PRO cable instrumentation (Guideline Geo, 2022) in 2018 and 2019 and Omnirecs DATA-CUBE (DiGOS, 2024) standalone stations in 2021 and 2022. This approach allowed for the removal of non-linear noise from the raw data in the later vertical stacking process.

The study site was also investigated using a shallow electromagnetic survey and monitoring. The Frequency Domain Electromagnetic Method (FDEM) is an electromagnetic technique that uses its own electromagnetic (EM) source to measure the resulting EM field close to the ground (Tabbagh, 1986). Measurements were carried out once in 2022, utilising the CMD-MiniExplorer 6L equipment from the Czech company GF Instruments (GF Instruments, 2024). This device allows for the simultaneous measurement of apparent electrical conductivity at six different depths, ranging approximately from 0.25 m to 2.3 m below the ground surface.

The FDEM measurement system comprises both a transmitter and receiver coil. Both coils lie on the same plane and have identical alignments, which can be either vertical or horizontal. The coils are positioned at a set distance apart, known as spacing. The transmitter coil produces a primary magnetic field that induces eddy currents in the ground. These eddy currents, in turn, create a secondary magnetic field. The receiver coil detects this secondary field. The strength of the detected signal is indicative of the average electrical conductivity (or electrical resistivity) of the medium the secondary field passes through. Therefore, the recorded data provides valuable information about the subsurface electrical conductivity (Kamm et al., 2013; McNeill, 1980). A survey grid was designed for dense coverage of the slope, featuring parallel profiles that spanned the landslide. These profiles varied in length and were spaced at distances ranging from 4 to 6 m. We adopted the CMD-MiniExplorer 6L's VD variant for our study, a device celebrated for its distinctive ability to facilitate concurrent measurements with six distinct depths of investigation. These depths, specifically 25, 50, 80, 110, 160, and 230 cm, were deliberately selected based on in-depth geological considerations. This type of device is called a multilevel conductivity meter (Beamish, 2011). A continuous mode was employed for the measurement process, operating with a time step of just one second. Alongside this, positioning was achieved through a GPS antenna, ensuring a positioning accuracy of approximately 1 m. To optimise data collection, the marching time was calibrated so that the measurement interval along the profile was consistent at about 1 m.

The survey covered the entire slope area, excluding only its highest part near the buildings, which was omitted due to strong interference present in that area (Fig. 3). The rest of the slope was surveyed using

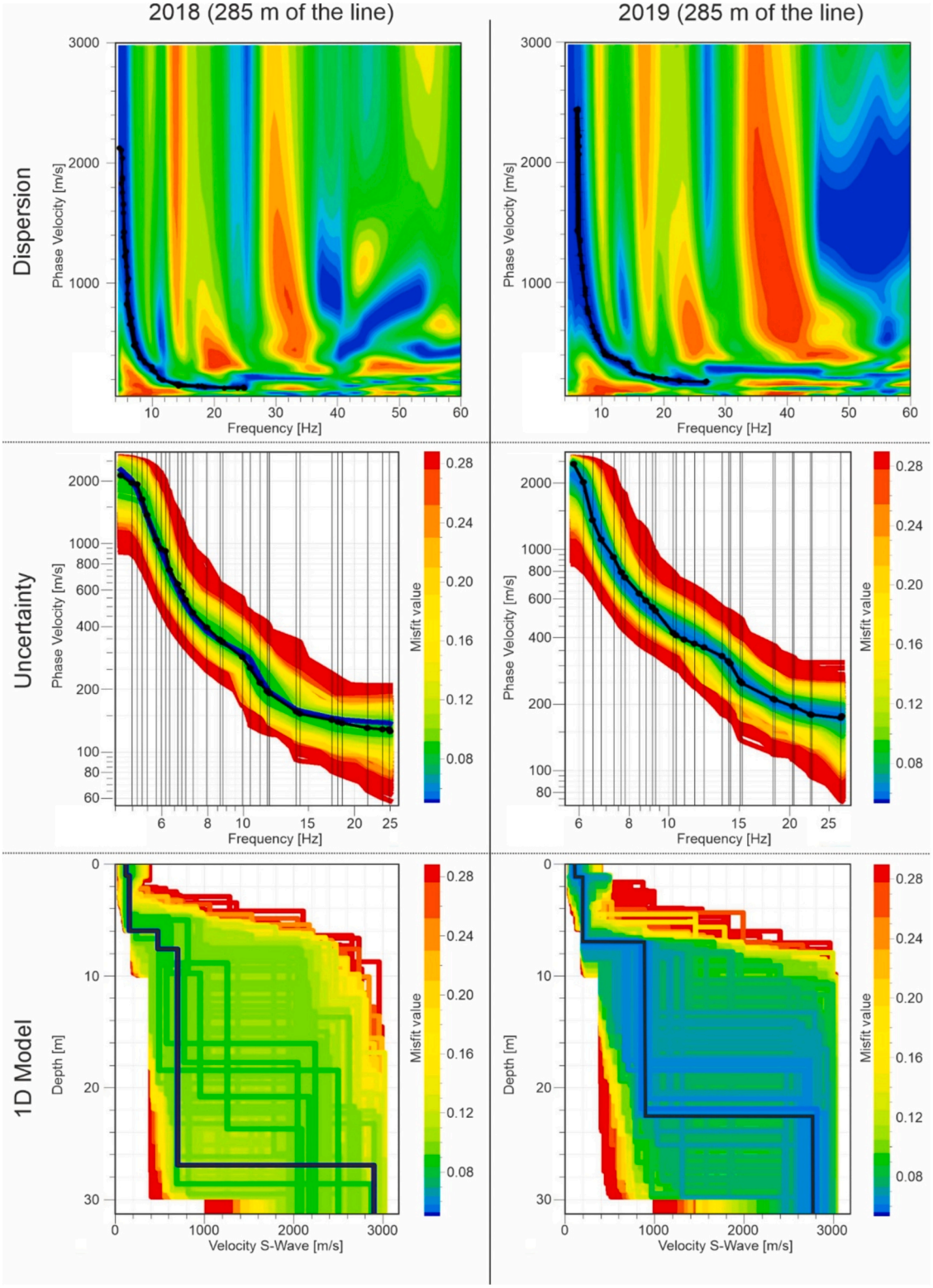

Fig. 6. Comparison of MASW results and observed soil movement in years 2018–2019. The dispersion characteristics are changed and shifted towards higher frequencies in later data. The best models are marked with solid black lines.

densely spaced profiles. Locally, the measurement grid was intensified with perpendicular profiles along the slope, especially in the central part where a landslide niche was present and in areas where surface water appeared at the bottom of the slope. The measurement step on the profiles was approximately 1 m, while the distance between profiles did not exceed 4 m. The measurement grid was established using surveying rods, and the position of the measurement points was further determined using the device's built-in GPS antenna with a precision of less than 10 cm on average both for coordinates and elevation.

Terrestrial laser scanning was performed using the RIEGL VZ 6000 (RIEGL, 2022) at four points to cover the entire sliding zone. Each scan operated at an effective rate of 222,000 measurements per second, with

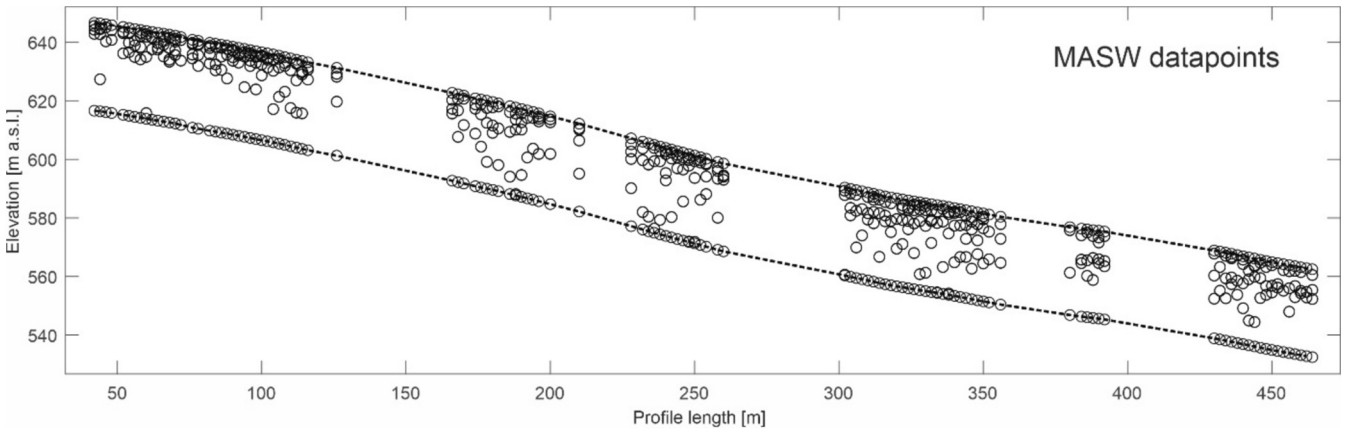

Fig. 7. Data points for the interpolation, after the rejection of high error values for the 2021 dataset.

an accuracy of 15 mm and precision of 10 mm. The Leica Viva GPS RTK system, connected to the GNSS reference ASG-EUPOS station in Żywiec, Poland, measured the position of each TLS point, reducing positioning errors to less than 10 cm. This setup facilitated the creation of detailed DTM models with a resolution of at least 0.1 m.

3. Data processing

3.1. Multichannel analysis of surface waves

The method employed enabled the identification of the shallowest zone, including residual zones and low-velocity layers. To effectively determine dispersion curves in a reproducible manner, data from four years of observations were pre-processed consistently. In each case, manual excision of the refraction data (front mute) and bandpass filtering in the range of 2–4–60-62 Hz were applied. The seismic records were normalised in terms of amplitude, and individual shots were cut from common seg-y files and separated into individual shot gathers. The interpretation of the data was conducted using the Geopsy package (Version 3.4.2) (Wathelet et al., 2020). Since the purpose of using MASW analysis was to show both horizontal and temporal variability of the landslide, it was necessary to select an interpretation window with optimal dimensions. This aimed to maintain a reasonable depth range for geophysical reconnaissance while minimizing areas along the profile lacking geophysical information. The final shot offset was 10 m, which eliminated near-field effects. Each 1D model was based on 60 m segments cut from individual excitation records to obtain homogeneous profiles that could be assembled into a 2D image over the depth range of interest. This means that in the case of the 2018 and 2019 data, an area containing 12 geophones at each excitation point was interpreted, and in the case of the 2021 and 2022 data, 60. In addition, the signal time window was limited to 800 ms, which, in combination with the spatial interpretation window, allowed the elimination of far-field effects. As a result, consistent dispersion curves were obtained for individual excitations from each year, where the surface wave was well-developed and undisturbed by natural low-frequency seismic noise. Also, the number of 1D curves that were used to generate 2D models is optimally large, providing good interpolation results for one-dimensional models. Since the 2018 and 2019 data were excited every 5 m, and the 2021 and 2022 data were excited every 2 m, a significant compaction of the number of 1D models and, ultimately, the overall resolution of the data from the last two years is evident.

The generation of curves in Geopsy is based on the use of F-K transformations. Each curve was manually picked three times and averaged (Fig. 5). In this way, ranges of quilting inaccuracies were determined due to the precision of the person interpreting the data. This allowed this error to be taken into account during the inversion process.

Table 1
The key seismic data processing steps.

Number	Procedure	Parameters	Purpose
1	Pre-stack data quality control (QC)	Root mean square (RMS) > 1000 and manual data correction	Removal of bad data points across whole datasets
2	Vertical stacking	Diversity stack	Attenuation of random noise. Enhancing S/N ratio.
3	Post-stack data QC	Manual data correction	Removal of remaining bad traces from data
4	Geometry Building	SEG-Y headers filling and manipulation based on shot and receiver naming scheme. Merging data with GPS information	Correct shot-receiver positions across the gathering lines
5	Geometry QC	Manual QC of field data and SEG-Y headers	Removal of mistakes from GPS and geodetic calculations
6	Data filtration	Butterworth filtration (2–4–60-62 Hz)	Removal of refracted waves from data. General data filtration in expected frequency.
7	Front mute	Manually chosen date range	Removal of non-linear noise from P-wave first arrivals.
8	Data normalisation	Automatic gain control	Normalisation of the amplitudes
9	Dispersion curve modelling	60 m window and 10 m offset for each shot. F-K transformation technique for dispersion curves generation.	Visualisation of dispersion phenomena
10	Dispersion curves picking	3 times picking and averaging each dispersion curve	Obtaining precise and well-parametrized dispersion curves
11	Picked curves inversion	Inversion of dispersion curves, using general starting data for whole datasets. 50 Monte Carlo and 10,000 Nearest-neighbourhood models considered in the combined inversion approach.	Set of 1D models, processed using the same starting model so as not to bias the outcome – estimated uncertainty parameters.
12	Result interpolation into 2D model	A linear algorithm for interpolation and data regularisation across the 0.2 m vertical and 0.5 m horizontal scale grid. Rejection of high uncertainty 1D profiles.	2D profiles of the landslide near-surface zone

Table 2
Inversion parameters for MASW data for all years based on preliminary tests and results of previous studies.

Layer No.	VS range [m/s]	Thickness	Assumed VS faster than the previous layer
Layer 1	50–400	1–3	No
Layer 2	50–500	1–6	No
Layer 3	200–1000	1–10	No
Layer 4	400–2000	1–30	No
Layer 5 (Half-Space)	1000–3500	Infinity	Yes

The inversion itself was performed in the Dinver package, using a combination of Monte Carlo and nearest neighbour algorithms. After the inversion, the 1D profiles were evaluated in terms of data quality (Fig. 6). The average misfit values for all 1D profiles were: 2018–0.063; 2019–0.070; 2021–0.071; 2022–0.078. The dominant value was 0.06 for the best-fitting model for all years. As shown in Fig. 6, the theoretical dispersion curves follow the real ones across the frequency spectrum. The 1D curves with anomalous RMS values were rejected (Fig. 7). The final step was interpolation and normalisation of the data to prepare 2D cross-sections of the study site. Detailed information about processing steps and parameters is presented in Tables 1 and 2.

3.2. Unsupervised machine learning for MASW data

Unsupervised machine learning methods in near-surface geophysics applications can be used to assess the condition of subsurface structures, including grouping data (Russo and Athanasopoulos-Zekkos, 2024), detecting zones with common features (Ward et al., 2014) or facilitating identification of changes (Delforge et al., 2021). Compared to supervised methods, unsupervised algorithms, such as K-means clustering, are a more realistic alternative when labelled seismic data are limited. Additionally, these methods are less dependent on the quality of labelled data, making them an efficient tool for quickly tagging and analysing geophysical data. However, K-means clustering has limitations, including its reliance on the assumption of Gaussian distribution of data and its sensitivity to noise. The method also requires the number of clusters to be pre-defined, which can be subjective and vary based on data complexity (Xia et al., 2018).

The K-Means algorithm employed clusterization to integrate multiple data from each MASW result that normally are omitted. Information on shear wave velocities (V_S), and uncertainties of depth and velocities, as well as picking precision, was integrated for enhancing 2D models. The integration of data through clustering yields more precise and numerically consistent outcomes (Merghadi et al., 2020; Whiteley et al., 2021b). The K-means algorithm iteratively aims to divide the dataset into K pre-defined, separate subgroups, ensuring each data point belongs to only one cluster. Its objective is to maximise the similarity of data points within each cluster while minimizing the dissimilarity between them. This is achieved by assigning data points to clusters in a manner that minimises the sum of squared distances between the data points and their respective cluster centroids. The clustering process was executed using the SciKit Learn package (Pedregosa et al., 2011) in the Python programming language. The initial number of clusters was set to 5, based on the prior data from initial studies (Marciniak et al., 2021) and information from MASW outcomes. After testing multiple algorithms, the K-means approach proved to be most useful in the presented case study, enhancing the visibility of changes in zones, where on the surface largest variations are observed.

3.3. Frequency domain electromagnetic method

We embarked on a meticulous sorting and filtering methodology during a phase in which the gathered data underwent a thorough and systematic review, crucial for isolating and eliminating anomalies, especially individual spikes (Table 3). This ensured that the subsequent analyses were conducted with the most reliable data set possible. After this rigorous refinement, the data were subjected to a 1D inversion process using the Occam algorithm (Constable et al., 1987), known for its efficiency in addressing complex geophysical inversion tasks (Klityński et al., 2019, 2020). The objective was to apply qualitative interpretation foundations to the data management and analysis processes.

Table 3
Interpretation scheme for EM data.

Number	Procedure	Parameters	Purpose
1	Selection of soundings	Multiple measurements in one place Strong interference	Rejection of those soundings that were strongly disturbed or sharply deviated from the trend at all depths. In addition, single soundings in larger groupings were selected.
2	1-D Occam Inversion	Starting model: Homogeneous halfspace with 100 Ωm Number of layers: 30 Minimum Depth: 0.1 m Maximum Depth: 5 m Number of iterations: 30	A 1D model was calculated for each survey point using the Occam algorithm. The final result is a smooth model that corresponds to the measurement curve. Most of the obtained models were fitted with an RMS of less than 5 %. Those curves for which a fit with an RMS of less than 10 % was obtained were discarded from further analysis.
3	Depth selection	Selected depths: 30 cm, 50 cm, 80 cm, 110 cm, 160 cm, 230 cm	From the resulting 1D models for each measurement point, the values of the calculated resistivities for the depths corresponding to the obtained apparent conductivities during the measurement were cut out.
4	Interpolation	Kriging with linear variogram	Kriging is a geostatistical method for spatial interpolation, predicting values at unmeasured locations using spatial correlation among data points.
5	Map presentation	Colour relief map	Colour relief maps are raster-based and utilise grid files to depict Z values, such as resistivities, using colours chosen by the user.

During the inversion process, a nuanced approach was taken where each data point was given its due attention. Instead of bundling them together as a collective set, every point was processed as a standalone sounding. This methodology underscores each data fragment's inherent value and distinct significance. Once this inversion stage was completed, a methodical interpolation of the data followed. This step was fundamental in facilitating the generation of detailed resistivity distribution maps. It is worth noting that these maps were meticulously fashioned to be consistent with the sounding depths that were previously employed to measure apparent conductivity.

The verification of faulty data for the FDEM (Frequency-Domain Electromagnetic Method) was conducted in two stages: the first step involved identifying and removing measurement points where negative conductivities were observed or points exhibiting extremely high conductivity values on a single channel without a preceding gradual increase. During the second stage, if the fit during the 1D inversion process did not meet the RMS (Root Mean Square) criterion of less than 5 %, the individual measurement point was removed from further processing. These steps aimed to improve data quality and ensure that only reliable measurement points were used in further analyses.

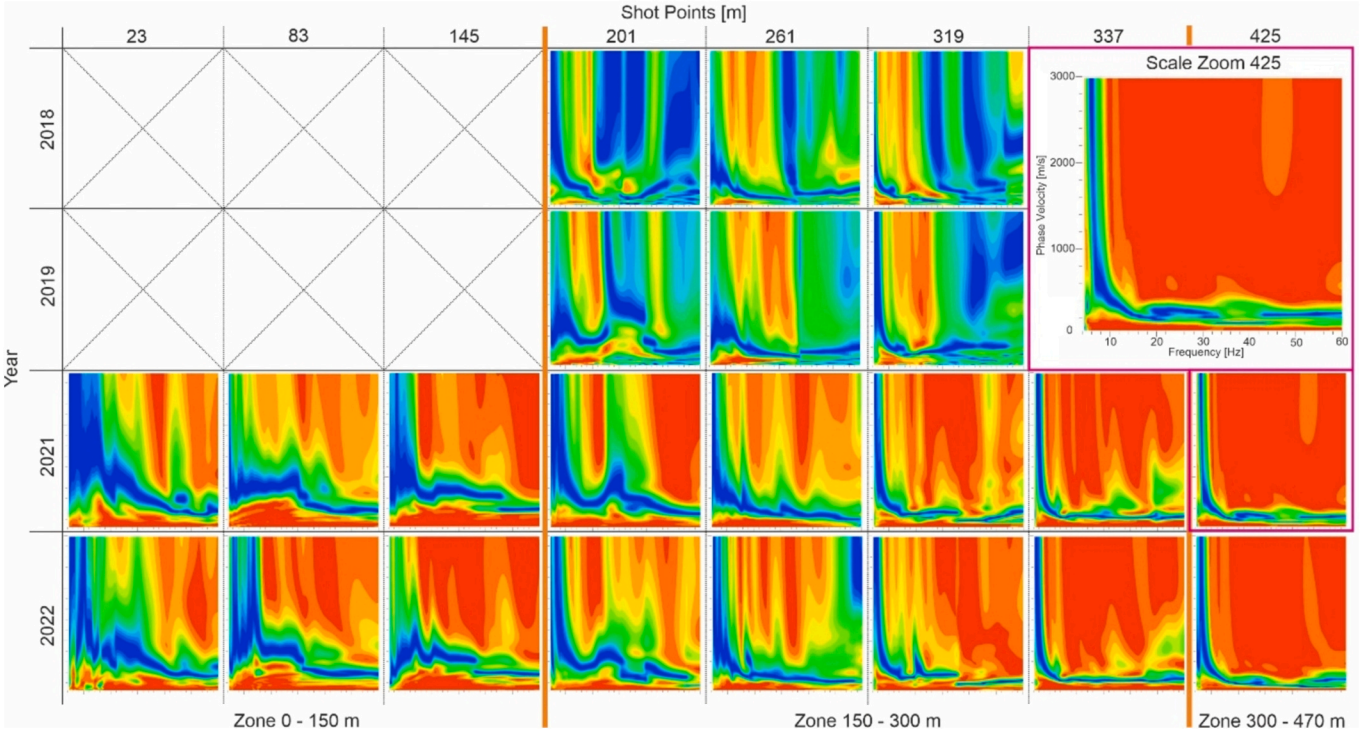

Fig. 8. Dispersion curve characteristic changes across the profile. The time-lapse comparison reveals strong spatial and time changes in the dispersion curve pattern.

4. Results and discussion

As a result of MASW and electrical conductivity data analysis, it was possible to identify several structures close to the surface. This finding holds particular significance when compared to previous studies, where the slip plane was depicted without distinction of the exact changes occurring within the landslide body (Marciniak et al., 2021; Wróbel et al., 2023). Since in the cited example, the shallow layer somehow determines the response of the entire medium to conditions occurring at depth, understanding its evolution is critical in the case under study with a large anthropogenic influence. The surface layer is pivotal in regulating the infiltration of water, particularly rainwater, into the deeper layers of the landslide. A highly permeable surface layer would facilitate rapid saturation of the slope. To better understand the changes in the landslide, remote sensing observations (DEM from May 2019) were correlated with geophysical data, specifically from the MASW method. This shows several blocks in colluvium with recognized slipping surfaces between them, that are visible at the surface as discontinuities.

4.1. Multichannel analysis of seismic waves

Integrating single dispersion curves (Fig. 8) in 2D profiles using linear interpolation revealed a series of discontinuities that overlap block-wise.

These structures correlate well with observations on the surface (Fig. 9), enabling recognition of subblocks and confirming their occurrence in real structures. Due to measurement differences in the first two years of monitoring, not all discontinuities can be identified throughout the study period.

As with single curve observations, three zones along the profile can be highlighted. These are, in turn:

- 0–150 m – the zone in which we track the variation of the structure in the form of a single area of reduced velocity relative to the following year. This highlights the seasonal change in stress and the influence of artificial snow that caused an increase in ground compaction in this area during the winter, which explains the lack of visibility of this detachment in the June 2022 data. It cannot be ruled out that there was a shift and discharge of accumulated stresses in this area.
- 150–350 m – the main colluvium of the landslide, where we distinguish several discontinuities and rock blocks. A gradual pattern of soil compaction is observed here, as well as a change in the shape of the discontinuity. This zone illustrates the greatest time-dependent variability in the study area. From the data in the work of Wróbel et al. (Wróbel et al., 2023), surface observations of the ground indicate up to 2 m, year-to-year shifts in the study area. Since the structures are preserved, it should be assumed that the movement in the described zone is homogeneous, to which the effect of ground freezing and the mass of corrugated snow contributes. As the annual snow cover is 1 m at this location, this puts considerable pressure on this zone, which is not very compact due to movement-related ground disturbance. In addition, the extended retention period of snow, due to its stockpile, causes longer effects of the frost effect, and thus hydrological changes in the form of increased surface runoff along the ground surface have also been observed.
- 350–470 m of profile – a zone of relatively consistent structure, with changes resulting from soil moisture. The geological system is relatively unchanged in this area, especially at 450 m of the profile. However, changes in the parameters of the contact zone are noticeable. Since there is increased surface waterlogging in this area, which is also evident from the electrical conductivity data, this seems to indicate that the landslide formation has breached the boundary of the impermeable layers. The soil outflow occurring in this area is along the slip zone, starting at 320 m in the profile and extending to the surface for about 400 m. At the surface, this area is highly eroded by surface runoff.

Changes in S-wave velocities are observed in the central area, which is particularly evident in the contrast between velocities in 2018 and 2019. This suggests the strong dynamics in this area, which is undergoing increasing compaction due to the pressure of the above layers on the area that has previously shifted.

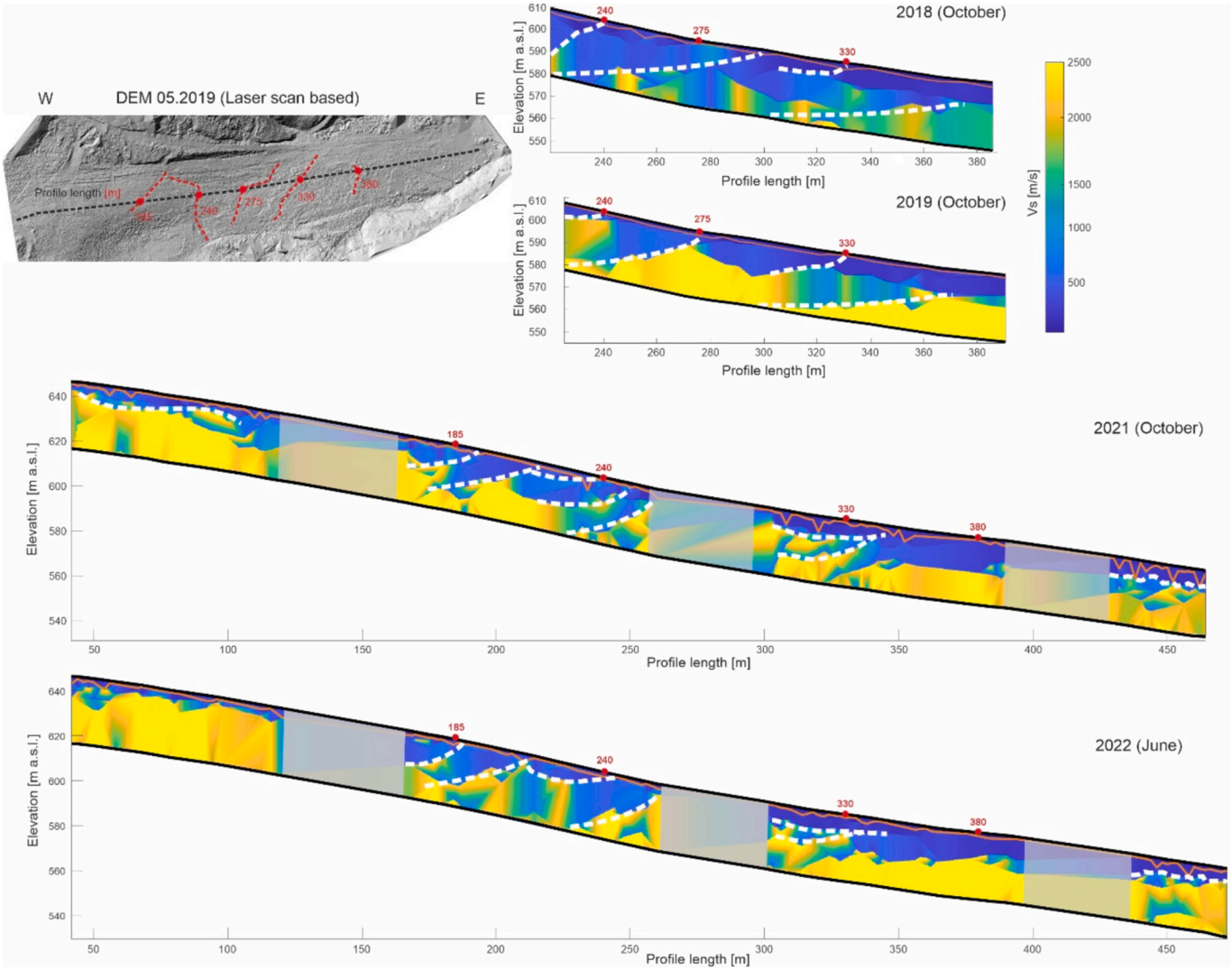

Fig. 9. The 2D seismic profile. The geophysical boundary shapes are relatively similar, however, there is a clear difference in observed V_S velocity values. White dashed lines mark the main discontinuities visible over the years. Due to survey geometry and interpretation schemes, grey polygons mark areas lacking data. The red dots indicate the discontinuities visible on the surface (DEM). (For interpretation of the references to colour in this figure legend, the reader is referred to the web version of this article.)

To better illustrate the changes in the landslide, data clustering was performed using the K-means algorithm (Fig. 10). For this purpose, a series of data on measurement uncertainty, the uncertainty of determining individual boundaries, the uncertainty of velocity estimation, as well as the resultant values themselves were utilized to enhance imaging quality by incorporating additional parameters. Since not only the result parameters but also the intermediate values describing them are dependent on the studied structure and its variability over time, their use represents an increase in the data density and type on which the interpretation model is based. This approach highlights the variability, especially in the area below the overlying near-surface zone. The detailed interpretation is visible in Table 4.

The largest changes are observed between the years 2018 and 2019, where the area of cluster number 3 increases. The area closest to the surface is relatively unchanged over time, with a similar pattern from year to year. However, large changes can be seen for the 50–150 m zone in 2021–2022, where in 2021, the boundary between cluster 0 and clusters 2, 3 and 4 is very heterogeneous. It indicates a very high variability of parameters in this zone, which was also noted in the data for the S-wave velocity speed itself. The clustering result also illustrates the slight variability of the area between 320 and 450 m of the profile. The result in Fig. 8 highlights the variability below the overlap zone (the near-surface zone with cluster number 0) in a much larger way while preserving the shape followed by the movement in the described area. Analysis of the seismic data, both in the form of images of individual curves, as well as 2D cross sections and clustering results, emphasizes significant variation in the landslide colluvium. Previous studies indicate that the slip zone is located at a depth of 35 m (Marciniak et al., 2021). The presented results supplement this knowledge with information about the movement of individual blocks. The imaged velocity values over the entire length of the profile indicate a homogeneous structure of the shallowest layer (0–10 m) and deeper rock structures. However, the variability of layers below 10 m depth in the form of increased ground compaction as a result of sliding of ground masses in particular years is apparent, which is also evident in the comparison of the course of sliding, especially on the long profiles from 2021 to 2022.

4.2. *Frequency domain electromagnetic method*

To compare the results obtained by the FDEM method to the seismic results, a resistivity profile was produced for the first 3 m below the surface. The data were treated with a 1D inversion, prior to which it was

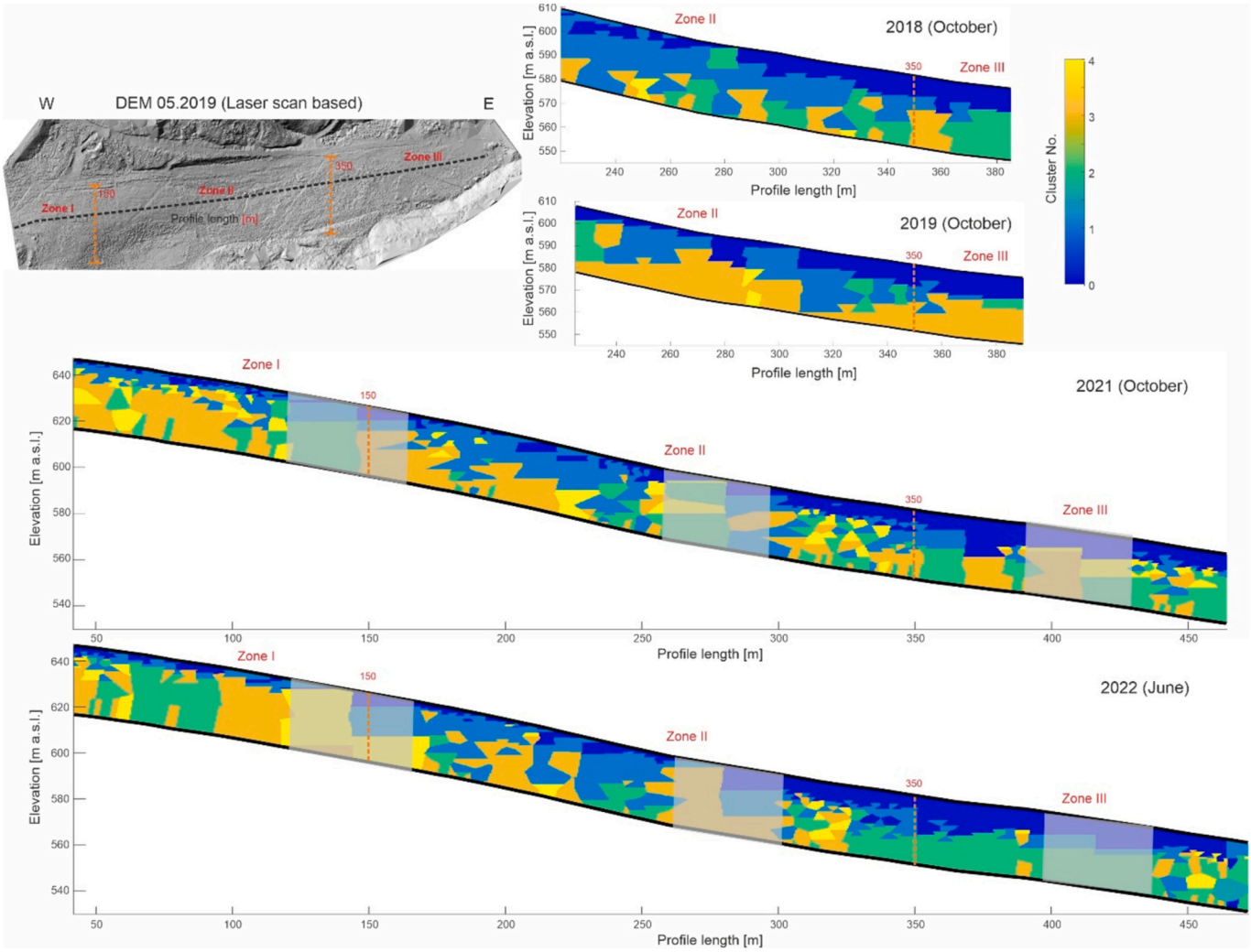

Fig. 10. The 2D result of the ML approach using the K-means algorithm. In comparison to the standalone approach, where the model is based only on a single parameter, adding information about uncertainties significantly enhances the visibility of zones with the largest changes. Based on the observed changes, three zones with different characteristics were distinguished (orange dashed lines).

Table 4
Qualitative analysis and interpretation of clustered data.

Cluster Number	Compaction	Water saturation	Geological composition
0	Very low	High	Sands, gravels and clays mix
1	Low	Very high	Clays
2	Medium	Low	Shales
3	High	Low	Sandstone complex
4	Very high	Low	Sandstone complex

necessary to convert conductivity to resistivity, hence the presentation of the results on a resistivity scale. This profile (Fig. 11) was obtained by interpolating the 1D inversion results for measurement points on or near the seismic profile. The depth scale is overlain ten times, with the elevation scale on the left and the actual depth scale on the left.

There is a marked difference in resistivity between the upper and lower parts of the slope, which was expected. However, the local reductions in resistivity in the upper and middle parts of the studied slope, around 150 and 200 m of the profile, are much more interesting. The shallowest layer (approximately 20 cm below the ground surface) is highlighted in red. Since the measurements were taken when it was very dry, it can be assumed that the pore space is filled with air. Hence, the high resistivities of the first layer strongly affect the shape of the model.

Resistivity distribution maps are shown for the six specific probing depths (Fig. 12). Two distinct zones are apparent in the electrical conductivity measurement results. Firstly, a noticeable zone of higher resistivity is situated in the western part of the study area, which corresponds to the upper region of the slope. Secondly, the opposite can be observed in the lower section of the slope, specifically in the eastern section of our study area, where there is a pronounced zone of lower resistivity. Furthermore, a corridor of exceptionally low resistivity can be distinctly seen extending across the study region from northwest to southeast, becoming particularly conspicuous at greater depths. At depth, the contrast between these two zones becomes even more pronounced, suggesting variations in the subsurface materials and structures. The distribution of highly electrically conductive materials in the lower slope segment is a hallmark of colluvium deposits. Regrettably, the method's depth limitations prevent us from precisely determining the parameters associated with potential landslides. However, this methodology does provide the capability to correlate shallow layers with the ERT method. The considerable depth of the aeration zone may be responsible for the extremely high resistivity of the near-surface layers. Measurements were made under dry conditions. It is also important not to overlook other factors that could contribute to the high resistance in the shallow zone, including fissuring, ground disturbance, increased porosity, and a decrease in compaction, among others. Nevertheless, locating the most waterlogged area along which rainwater

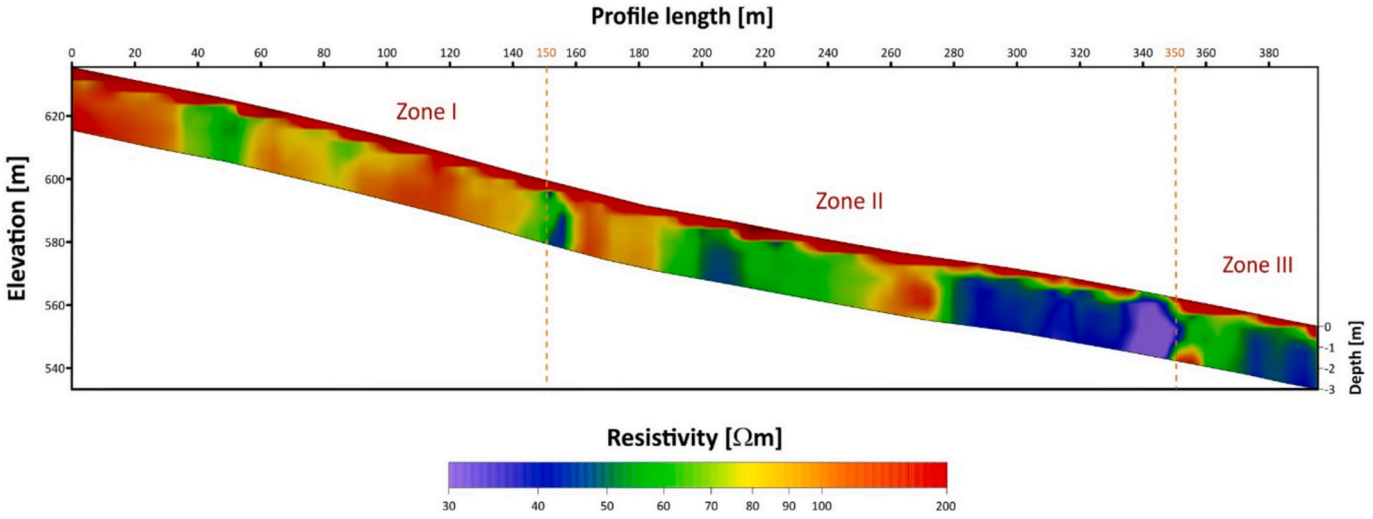

Fig. 11. Map of Resistivity Distribution along the seismic profile. The orange dashed line presents the border between different zones, which were distinguished based on V_S (Fig. 9) and clustered data (Fig. 10). The resistivity distribution confirms zone differentiation, with noticeably different values across each zone at the depth below
1 m.

transports was most likely possible. This is a clearly visible zone of extremely low resistivity.

Moreover, we also present data regarding the normalised in-phase parameter. This parameter is graphically represented in (Fig. 13). Peak values are predominantly clustered in the northern segment of the study area and strongly correlate with the zones marked by extremely low resistivity. When observing the in-phase distribution maps, particularly for the deeper depth ranges, it's evident that the highest values of this parameter predominantly dictate the overall distribution pattern. An intriguing finding is that elevated in-phase values might directly correlate with the infrastructure related to an active ski slope. While the measurements under discussion were procured during the summer months – a period when the ski slope remains dormant – the infrastructure associated with the ski operations remains fully intact and in place. This infrastructure could potentially play a role in influencing the observed values, thus warranting further investigation.

In analysing the resistivity distribution image and in-phase, the existing ski infrastructure on the slope should be kept in mind. It can be concluded with a high degree of probability that the linear anomaly in the southern part of the study area is related to the presence of a small ski lift. Similarly, there is a strong local anomaly in the northern part of the area, which can be related to the metal poles supporting the lift. The dominance of anomalies related to ski infrastructure in the resistivity picture cannot be ruled out. Still, a two-zone pattern is nevertheless apparent – clearly high resistivity at the top of the slope and low resistivity at the bottom.

4.3. General overview

The analysis of data obtained through different methodologies reveals a noticeable relationship between very slow velocities in the shallow layers at the bottom of the slope and areas of low electrical resistivity spanning almost the entire depth investigated by the GCM survey. While it is somewhat more challenging to draw comparisons for the upper slope region, it is noted that higher resistivity levels are prevalent in layers extending from the surface down to 230 cm. Additionally, a comparatively thinner layer of low resistivity is observed in the upper section of the slope, highlighting the complex interplay between geological features and their electrical properties across different depths. The electrically low resistive and slow V_S characterized the area in the eastern part, which can be identified as having the greatest thickness colluvium with very high water content and shallow water table. In this part, there is even subsurface water flow periodically breaking to the surface. Furthermore, the study also uncovers a distinct correlation between the 'in-phase' parameter and geological characteristics in the lower segment of the slope. Here, its higher values coincide with zones of low resistivity and areas exhibiting slow seismic velocities, underscoring a pronounced low resistivity anomaly. This anomaly is strongly associated with the presence of substantial water volumes, suggesting a substantial hydrological influence. Notably, the elevated 'in-phase' values are likely to be linked to the ski infrastructure in the northern part of the slope. Despite the distance from these facilities at which the measurements were conducted, the potential impact of the ski infrastructure is evident in the presented maps, indicating its non-negligible effect on the area's geophysical properties. Correlating the geophysical data with geological information and observations from previous work (Marciniak et al., 2021; Wróbel et al., 2023), a clear division between the sandstone layers near the surface and the shale and sandstone complex forming the colluvium becomes apparent in the S-waves velocity profiles. This is reflected in the elevated resistivity values in the upper section of the landslide, compared to much lower values in its lower part. In addition, this is also demonstrated in the variable thickness of the low-velocity near-surface layer in the MASW results. The observed picture, alongside reduced compaction and variable water saturation of the massif, is influenced by the uniform structure of the upper part of the landslide, which has not yet undergone mass movements. Accordingly, the near-surface layer of sandstones has not been significantly affected, being characterized by high compactness and low porosity.

5. Conclusions

As one of the key geohazards in southern Poland, landslides represent a significant research focus, given their complex genesis and susceptibility to external factors, particularly amidst increasing urbanization and climate change. Understanding the triggering mechanisms is crucial in this context, especially as traditional approaches relying only on remote sensing and surface observations may no longer suffice in an era of advancing geohazard prediction and modelling capabilities.

Our findings demonstrate the possibility of improving the analysis of the variability of the zone most susceptible to natural and anthropogenic

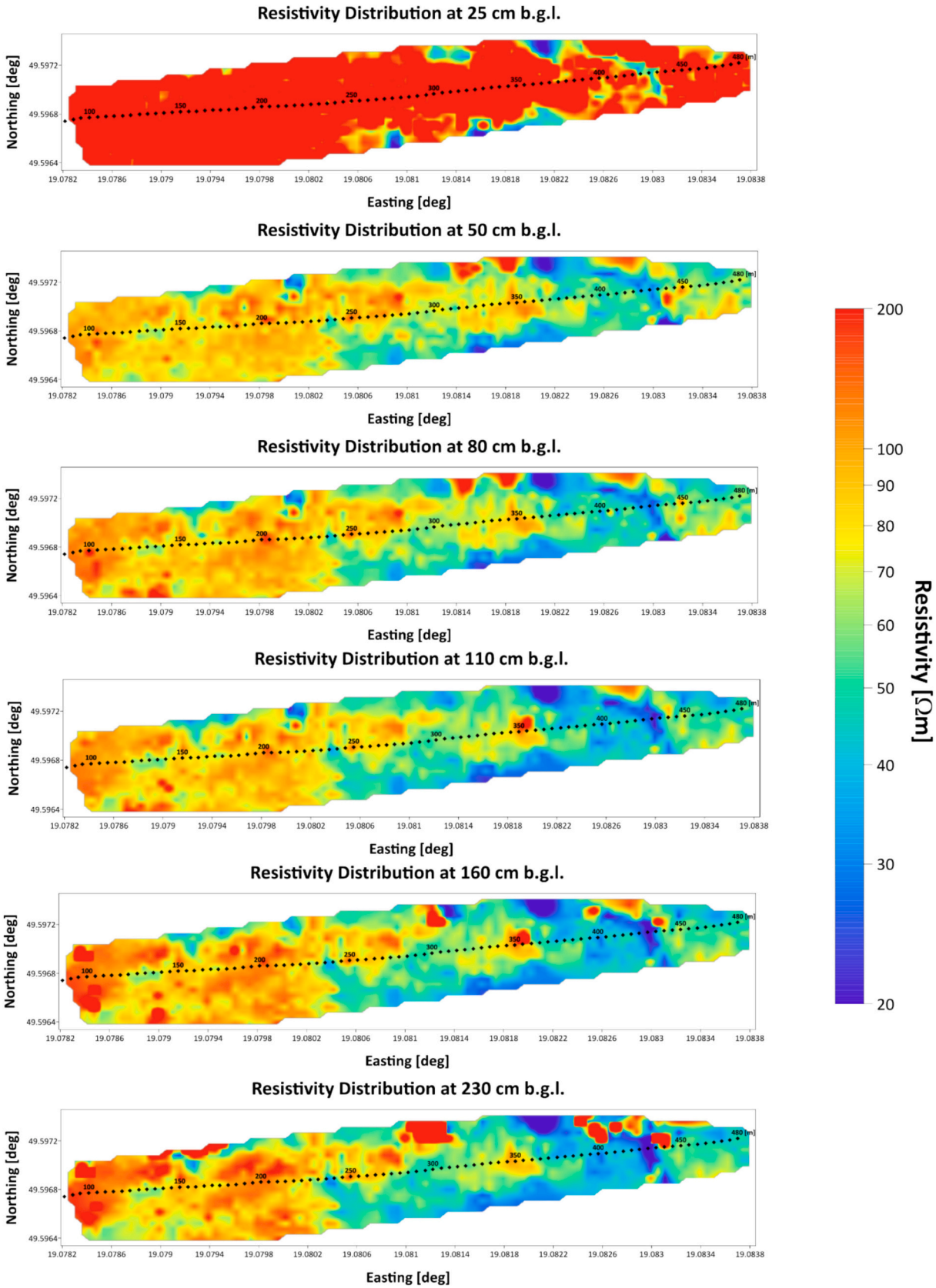

Fig. 12. Map of Resistivity Distribution at six different depths. Depth cross sections obtained from the conductivity method highlight the different distribution of geophysical parameters (electrical resistivity) for different parts of the study area. The course of the seismic profiles is marked with a dashed line along with the corresponding length.

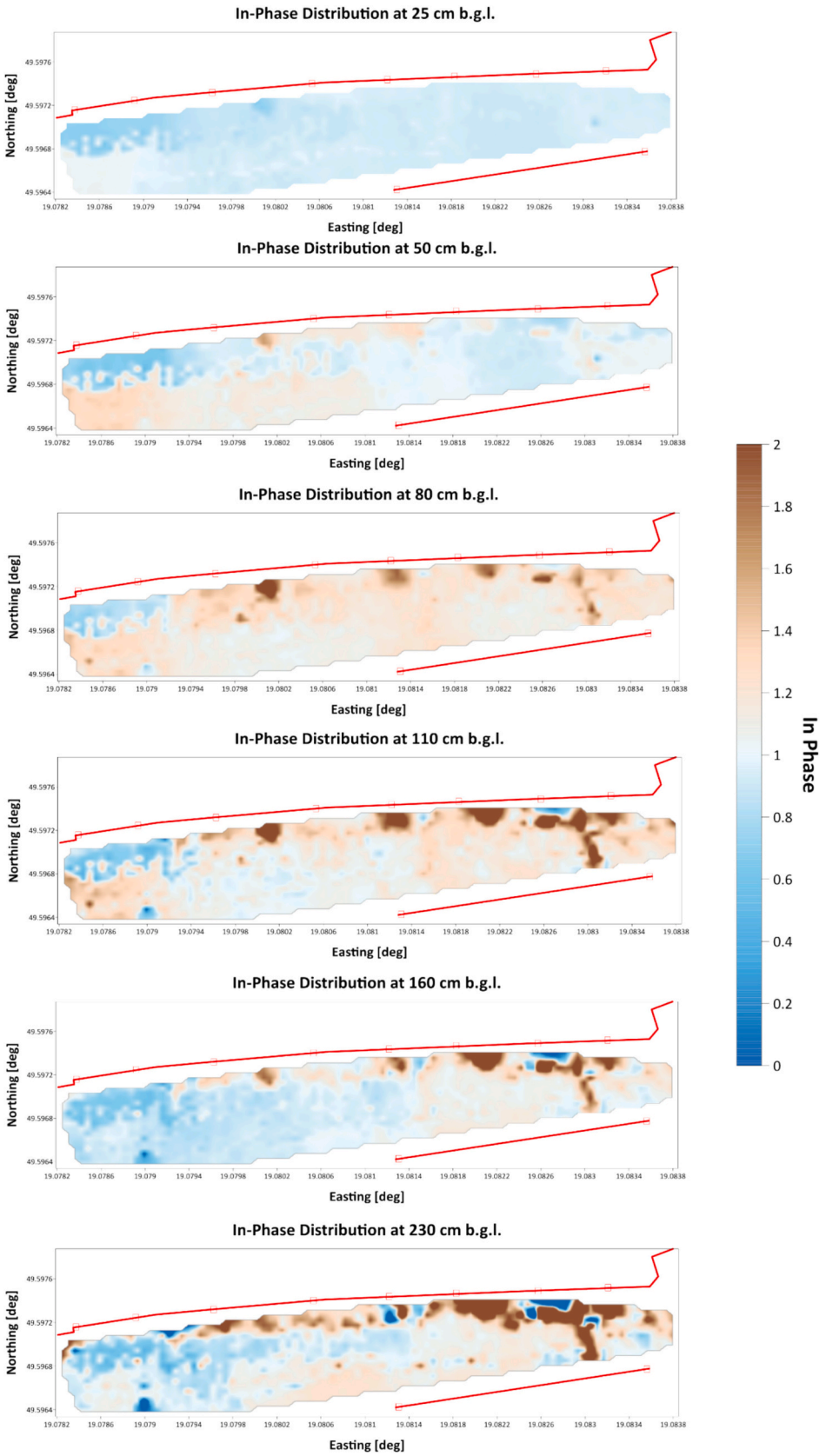

Fig. 13. Map of In-Phase Distribution at six different depths. The red line indicates the electrical infrastructure associated with the operation of the ski slope. (For interpretation of the references to colour in this figure legend, the reader is referred to the web version of this article.)

factors. In this area, notable changes in the form of ground freezing and fluctuating water saturation, exacerbated by the use of the area as a ski slope loaded with artificial snow, are observed.

This is especially evident in the velocity of S-type seismic waves, which are susceptible to settlement, specifically in response to alterations in ground compaction. Complementing this information is data from the conductivity method, which illustrates spatial changes in ground conductivity within the first 2 m. This elucidates the spatial distribution of the landslide and the differing interactions of natural and anthropogenic factors with the studied area.

The final interpretation, aided by integrating the results using unsupervised machine learning, reveals a homogeneous structure of the shallowest geological layer and its boundary, but with significant variability in individual parameters along the length of the profile. Seasonal variations further underscore the dominant influence of anthropogenic factors in the landslide's evolution.

This research is a unique example and one of the few such experiments that attempted to determine the impact of natural and anthropogenic factors on the area of ski slopes. Such findings serve as a valuable reference for understanding the anticipated changes in slope loading, particularly in the context of ongoing urbanization and development. Thus, this study serves as a meaningful large-scale model, offering insights into the potential outcomes of similar geoengineering applications.

CRediT authorship contribution statement

Artur Marciniak: Writing – review & editing, Writing – original draft, Visualization, Validation, Supervision, Software, Project administration, Methodology, Investigation, Funding acquisition, Formal analysis, Data curation, Conceptualization. **Sebastian Kowalczyk:** Writing – original draft, Software, Resources, Investigation. **Szymon Oryński:** Writing – original draft, Visualization, Software, Resources, Methodology, Investigation. **Justyna Cader:** Writing – review & editing, Writing – original draft, Visualization, Validation, Formal analysis. **Jonathan Chambers:** Writing – review & editing, Validation. **Iwona Stan-Kłeczek:** Writing – original draft, Software, Resources, Investigation. **Mariusz Majdański:** Writing – review & editing, Writing – original draft, Validation, Software, Resources, Funding acquisition.

Declaration of competing interest

The authors declare that they have no known competing financial interests or personal relationships that could have appeared to influence the work reported in this paper.

Data availability

Data will be made available on request.

Acknowledgements

We thank Brij Singh, Bartosz Owoc, Andrzej Górszczyk, Wojciech Gajek, Małgorzata Wróbel, Tomasz Gontar and Mariusz Chmielewski for helping during data acquisition.

This research was funded by the National Science Centre, Poland (NCN), grant numbers 2020/37/N/ST10/01486 and 2022/45/B/ST10/00658.

References

Altdorff, D., Galagedara, L., Nadeem, M., Cheema, M., Unc, A., 2018. Effect of agronomic treatments on the accuracy of soil moisture mapping by electromagnetic induction. CATENA 164, 96–106. https://doi.org/10.1016/j.catena.2017.12.036.

Amatya, P., Kirschbaum, D., Stanley, T., Tanyas, H., 2021. Landslide mapping using object-based image analysis and open source tools. Eng. Geol. 282, 106000. https://doi.org/10.1016/j.enggeo.2021.106000.

Anbalagan, R., Chakraborty, D., Kohli, A., 2008. Landslide hazard zonation (LHZ) mapping on meso-scale for systematic town planning in mountainous terrain. J. Sci. Ind. Res. (India). 67, 486–497.

Arbanas, S.M., Arbanas, Ž., 2014. Landslides: A guide to researching landslide phenomena and processes. In: Gaurina-Medjimurec, N. (Ed.), Handbook of Research on Advancements in Environmental Engineering. IGI Global, Hershey, PA, pp. 474–510. https://doi.org/10.4018/978-1-4666-7336-6.ch017.

Aslan, G., Foumelis, M., Raucoules, D., De Michele, M., Bernardie, S., Cakir, Z., 2020. Landslide mapping and monitoring using persistent scatterer interferometry (PSI) technique in the French alps. Remote Sens. 12. https://doi.org/10.3390/RS12081305.

Beamish, D., 2011. Low induction number, ground conductivity meters: a correction procedure in the absence of magnetic effects. J. Appl. Geophys. 75, 244–253. https://doi.org/10.1016/j.jappgeo.2011.07.005.

Bichler, A., Bobrowsky, P., Best, M., Douma, M., Hunter, J., Calvert, T., Burns, R., 2004. Three-dimensional mapping of a landslide using a multi-geophysical approach: the Quesnel Forks landslide. Landslides 1, 29–40. https://doi.org/10.1007/s10346-003-0008-7.

Constable, S.C., Parker, R.L., Constable, C.G., 1987. Occam's inversion: a practical algorithm for generating smooth models from electromagnetic sounding data. Geophysics 92, 289–300. https://doi.org/10.1190/1.1442303.

Crawford, M.M., Bryson, L.S., Woolery, E.W., Wang, Z., 2018. Using 2-D electrical resistivity imaging for joint geophysical and geotechnical characterization of shallow landslides. J. Appl. Geophys. 157, 37–46. https://doi.org/10.1016/j.jappgeo.2018.06.009.

de Jong, C., Carletti, G., Previtali, F., 2015. Assessing impacts of climate change, ski slope, snow and hydraulic engineering on slope stability in ski resorts (French and Italian Alps). In: Lollino, G., Manconi, A., Clague, J., Shan, W., Chiarle, M. (Eds.), Engineering Geology for Society and Territory, Vol. 1. Springer, Cham, pp. 51–55.

Delforge, D., Watlet, A., Kaufmann, O., Van Camp, M., Vanclooster, M., 2021. Time-series clustering approaches for subsurface zonation and hydrofacies detection using a real time-lapse electrical resistivity dataset. J. Appl. Geophys. 184, 104203. https://doi.org/10.1016/j.jappgeo.2020.104203.

DiGOS, 2024. Seismic Data Recorder DATA-CUBE^3 - User Manual [WWW Document]. URL https://digos.eu/CUBE/DATA-CUBE-User-Manual-2017-06.pdf (accessed 4.6.24).

Ding, W., Wang, G., Yang, Q., Xu, Y., Gao, Y., Chen, X., Xu, S., Han, L., Yang, X., 2023. Risk assessment and control of geological hazards in towns of complex mountainous areas based on remote sensing and geological survey. Water 15, 3170. https://doi.org/10.3390/w15183170.

Flores Orozco, A., Bücker, M., Steiner, M., Malet, J.P., 2018. Complex-conductivity imaging for the understanding of landslide architecture. Eng. Geol. 243, 241–252. https://doi.org/10.1016/j.enggeo.2018.07.009.

Furuya, G., Katayama, T., Suemine, A., Kozato, T., Watanabe, T., Marui, H., 2013. Application of the newly frequency domain electromagnetic method survey in a landslide area. In: Margottini, C., Canuti, P., Sassa, K. (Eds.), Landslide Science and Practice: Volume 2: Early Warning, Instrumentation and Monitoring. Springer Berlin Heidelberg, Berlin, Heidelberg, pp. 169–175. https://doi.org/10.1007/978-3-642-31445-2_22.

Gallardo, L.A., Meju, M.A., 2004. Joint two-dimensional DC resistivity and seismic travel time inversion with cross-gradients constraints. J. Geophys. Res. Solid Earth 109, B03311. https://doi.org/10.1029/2003JB002716.

GF Instruments, 2024. CMD - Multidepth Electromagnetic Conductivity Meters [WWW Document]. URL http://www.gfinstruments.cz/ (accessed 5.5.24).

Godio, A., Strobbia, C., De Bacco, G., 2006. Geophysical characterisation of a rockslide in an alpine region. Eng. Geol. 83, 273–286. https://doi.org/10.1016/j.enggeo.2005.06.034.

Golonka, J., Waśkowska-Oliwa, A., 2007. Stratigraphy of the Polish Flysch Carpathians between Bielsko-Biała and Nowy Targ. Geol. Akad. Górniczo-Hutnicza im. Stanisława Staszica w Krakowie, 33, pp. 5–27.

Guideline Geo, 2022. ABEM Terraloc - instrument datasheet [WWW Document]. URL https://wwwguidelinegeoc.cdn.triggerfish.cloud/uploads/2017/07/ABEM-Terraloc-Pro-2-TechSpec-210823-web.pdf (accessed 5.20.24).

Hasan, M., Shang, Y., 2022. Geophysical evaluation of geological model uncertainty for infrastructure design and groundwater assessments. Eng. Geol. 299, 106560. https://doi.org/10.1016/j.enggeo.2022.106560.

Hussain, Y., Hamza, O., Cárdenas-Soto, M., Borges, W.R., Dou, J., Rebolledo, J.F.R., Prado, R.L., 2020. Characterization of Sobradinho landslide in fluvial valley using MASW and ERT methods. REM - Int. Eng. J. 73, 487–497. https://doi.org/10.1590/0370-44672019730109.

Jongmans, D., Hemroulle, P., Demanet, D., Renardy, F., Vanbrabant, Y., 2000. Application of 2D electrical and seismic tomography techniques for investigating landslides. Eur. J. Environ. Eng. Geophys. 5, 75–89.

Kamiński, M., Zientara, P., Krawczyk, M., 2021. Electrical resistivity tomography and digital aerial photogrammetry in the research of the "Bachledzki Hill" active landslide – in Podhale (Poland). Eng. Geol. 285. https://doi.org/10.1016/j.enggeo.2021.106004.

Kamm, J., Becken, M., Pedersen, L.B., 2013. Inversion of slingram electromagnetic induction data using a born approximation. Geophysics 78, E201–E212. https://doi.org/10.1190/GEO2012-0484.1.

Keiler, M., Schneiderbauer, S., Fuchs, S., 2023. Global change, related impact on natural hazard processes, and potential consequences in social-ecological mountain systems. In: Schneiderbauer, S., Pisa, P.F., Shroder, J.F., Szarzynski, J. (Eds.), Safeguarding Mountain Social-Ecological Systems: A Global Challenge: Facing Emerging Risks, Adapting to Changing Environments and Building Transformative Resilience in

Mountain Regions Worldwide. Elsevier, pp. 23–29. https://doi.org/10.1016/B978-0-12-822095-5.00004-8.
Klityński, W., Oryński, S., Nguyen Dinh, C., 2019. Application of the conductive method in the engineering geology: Ruczaj district in Kraków, Poland, as a case study. Acta Geophys. 67, 1791–1798. https://doi.org/10.1007/s11600-019-00335-w.
Klityński, W., Oryński, S., Chau, N.D., 2020. The potential use of ground conductivity meters to identify the location of seepages—case study of the maniów levee near krakow, Poland. Geosciences 10, 97. https://doi.org/10.3390/geosciences10030097.
Knapen, A., Kitutu, M.G., Poesen, J., Breugelmans, W., Deckers, J., Muwanga, A., 2006. Landslides in a densely populated county at the footslopes of Mount Elgon (Uganda): Characteristics and causal factors. Geomorphology 73, 149–165. https://doi.org/10.1016/j.geomorph.2005.07.004.
Kucharska, M., Kamiński, M., 2008. Registration card of the landslide (registration number 24-17-152-029130) in the village of Cisiec [WWW Document]. URL https://geoportal.pgi.gov.pl/portal/page/portal/SOPO/Wyszukaj3 (accessed 4.4.21).
Lapenna, V., Perrone, A., 2022. Time-lapse electrical resistivity tomography (TL-ERT) for landslide monitoring: recent advances and future directions. Appl. Sci. 12. https://doi.org/10.3390/app12031425.
Lapenna, V., Lorenzo, P., Perrone, A., Piscitelli, S., Rizzo, E., Sdao, F., 2005. 2D electrical resistivity imaging of some complex landslides in the Lucanian Apennine chain, southern Italy. Geophysics 70, 11–18. https://doi.org/10.1190/1.1926571.
Le Breton, M., Bontemps, N., Guillemot, A., Baillet, L., Larose, É., 2021. Landslide monitoring using seismic ambient noise correlation: challenges and applications. Earth-Sci. Rev. 216, 103518. https://doi.org/10.1016/j.earscirev.2021.103518.
Lebourg, T., Hernandez, M., Zerathe, S., El Bedoui, S., Jomard, H., Fresia, B., 2010. Landslides triggered factors analysed by time lapse electrical survey and multidimensional statistical approach. Eng. Geol. 114, 238–250. https://doi.org/10.1016/j.enggeo.2010.05.001.
Li, X., Cheng, J., Yu, D., Han, Y., 2023. Research on landslide hazard assessment in data-deficient areas: a case study of Tumen City, China. Acta Geophys. 71, 1763–1774. https://doi.org/10.1007/s11600-023-01057-w.
Lu, K., Li, F., Pan, J., Li, K., Li, Z., Wang, P., 2024. Structural characterization and attempted displacement interpretation of the Baishuihe landslide using integrated geophysical methods. Eng. Geol. 336, 107568. https://doi.org/10.1016/j.enggeo.2024.107568.
Marciniak, A., Stan-Kłeczek, I., Idziak, A., Majdański, M., 2019. Uncertainty based multi-step seismic analysis for near-surface imaging. Open Geosci. 11, 727–737. https://doi.org/10.1515/geo-2019-0057.
Marciniak, A., Kowalczyk, S., Gontar, T., Owoc, B., Nawrot, A., Luks, B., Cader, J., Majdański, M., 2021. Integrated geophysical imaging of a mountain landslide – a case study from the Outer Carpathians, Poland. J. Appl. Geophys. 191, 104364. https://doi.org/10.1016/j.jappgeo.2021.104364.
McNeill, J.D., 1980. Electrical Conductivity of Soils and Rocks, Technical Note TN-5. Geonics Ltd., Mississauga.
Merghadi, A., Yunus, A.P., Dou, J., Whiteley, J., Thaipham, B., Tien, D., Avtar, R., Abderrahmane, B., 2020. Earth-Science Reviews Machine learning methods for landslide susceptibility studies: a comparative overview of algorithm performance. Earth-Sci. Rev. 207, 103225. https://doi.org/10.1016/j.earscirev.2020.103225.
Oszczypko, N., Ślączka, A., Żytko, K., 2008. Tectonic subdivision of Poland: Polish Outer Carpathians and their foredeep. Prz. Geol. 56, 927–935.
Paul, Z., Ryłko, W., Tomaś, A., 1996. Outline of the geological structure of the western part of the Polish Carpathians (without Quaternary formations). Prz. Geol. 44, 469–476.
Pazzi, V., Morelli, S., Fanti, R., 2019. A review of the advantages and limitations of geophysical investigations in landslide studies. Int. J. Geophys. 2019, 2983087. https://doi.org/10.1155/2019/2983087.
Pedregosa, F., Varoquaux, G., Gramfort, A., Michel, V., Thirion, B., Grisel, O., Blondel, M., Prettenhofer, P., Weiss, R., Dubourg, V., Vanderplas, J., Passos, A., Cournapeau, D., Brucher, M., Perrot, M., Duchesnay, É., 2011. Scikit-learn: machine learning in python. J. Mach. Learn. Res. 12, 2825–2830.
PGI-NRI, 2023. Geological Map of Poland 1:50 000 [WWW Document]. Polish Geol. Inst. - Natl. Res. Inst. URL https://geologia.pgi.gov.pl/arcgis/apps/MapSeries (accessed 11.7.23).
Pistillo, D., Colica, E., Amico, S.D., Farrugia, D., Feliziani, F., Galone, L., Iannucci, R., Martino, S., 2024. Engineering geological and geophysical investigations to characterise the unstable rock slope of the sopu promontory (Gozo, Malta). Geosciences 14. https://doi.org/10.3390/geosciences14020039.
RIEGL, 2022. RIEGL VZ 6000 - instrument datasheet [WWW Document]. URL http://www.riegl.com/uploads/tx_pxpriegldownloads/RIEGL_VZ-6000_Datasheet_2020-09-14.pdf (accessed 4.5.24).
Rixen, C., Stoeckli, V., Ammann, W., 2003. Does artificial snow production affect soil and vegetation of ski pistes? A review. Perspect. Plant Ecol. Evol. Syst. 5, 219–230. https://doi.org/10.1078/1433-8319-00036.
Russo, B.M., Athanasopoulos-Zekkos, A., 2024. Exploration of feature engineering techniques and unsupervised machine learning clustering algorithms for geophysical data on levees. In: Geo-Congress 2024. Vancouver, pp. 454–463. https://doi.org/10.1061/9780784485347.046.
Ryłko, W., 2013. Detailed Geological Map of Poland 1:50 000. Sheet: Milówka 1029. Polish Geol. Inst. - Natl. Res. Inst.
Sabatakakis, N., Koukis, G., Mourtas, D., 2005. Composite landslides induced by heavy rainfalls in suburban areas: City of Patras and surrounding area, western Greece. Landslides 2, 202–211. https://doi.org/10.1007/s10346-005-0002-3.
Smail, T., Abed, M., Mebarki, A., Lazecky, M., 2022. Earthquake-induced landslide monitoring and survey by means of InSAR. Nat. Hazards Earth Syst. Sci. 22, 1609–1625. https://doi.org/10.5194/nhess-22-1609-2022.
Tabbagh, A., 1986. What is the best coil orientation in the slingram electromagnetic prospecting method? Archaeometry 28, 185–196. https://doi.org/10.1111/j.1475-4754.1986.tb00386.x.
Uhlemann, S., Chambers, J., Wilkinson, P., Maurer, H., Merritt, A., Meldrum, P., Kuras, O., Gunn, D., Smith, A., Dijkstra, T., 2017. Four-dimensional imaging of moisture dynamics during landslide reactivation. Case Rep. Med. 122, 398–418. https://doi.org/10.1002/2016JF003983.
United Nations, 2015. Sustainable Development Goals [WWW Document]. URL https://sdgs.un.org/goals (accessed 2.12.23).
Villacorta, S., Ubeda, J., Tatard, L., Diez, A., 2015. Proposal for climate change impact research in Western Central Andes of Peru. In: Lollino, G., Manconi, A., Clague, J., Shan, W., Chiarle, M. (Eds.), Engineering Geology for Society and Territory – Vol. 1: Climate Change and Engineering Geology. Springer, Cham, pp. 13–16. https://doi.org/10.1007/978-3-319-09300-0_3.
Vranken, L., Vantilt, G., Van Den Eeckhaut, M., Vandekerckhove, L., Poesen, J., 2015. Landslide risk assessment in a densely populated hilly area. Landslides 12, 787–798. https://doi.org/10.1007/s10346-014-0506-9.
Ward, W.O.C., Wilkinson, P.B., Chambers, J.E., Oxby, L.S., Bai, L., 2014. Distribution-based fuzzy clustering of electrical resistivity tomography images for interface detection. Geophys. J. Int. 197, 310–321. https://doi.org/10.1093/gji/ggu006.
Wathelet, M., Chatelain, J., Cornou, C., Di Giulio, G., Guillier, B., Ohrnberger, M., Savvaidis, A., 2020. Geopsy: a user-friendly open-source tool set for ambient vibration processing. Seismol. Res. Lett. 91, 1878–1889. https://doi.org/10.1785/0220190360.
Whiteley, J.S., Chambers, J.E., Uhlemann, S., Boyd, J., Cimpoiasu, M.O., Holmes, J.L., Inauen, C.M., Watlet, A., Hawley-Sibbett, L.R., Sujitapan, C., Swift, R.T., Kendall, J. M., 2020. Landslide monitoring using seismic refraction tomography – the importance of incorporating topographic variations. Eng. Geol. 268, 105525. https://doi.org/10.1016/j.enggeo.2020.105525.
Whiteley, J.S., Watlet, A., Kendall, J.M., Chambers, J.E., 2021a. Brief communication: the role of geophysical imaging in local landslide early warning systems. Nat. Hazards Earth Syst. Sci. 21, 3863–3871. https://doi.org/10.5194/nhess-21-3863-2021.
Whiteley, J.S., Watlet, A., Uhlemann, S., Wilkinson, P., Boyd, J.P., Jordan, C., Kendall, J. M., Chambers, J.E., 2021b. Rapid characterisation of landslide heterogeneity using unsupervised classification of electrical resistivity and seismic refraction surveys. Eng. Geol. 290, 106189. https://doi.org/10.1016/j.enggeo.2021.106189.
Wilkinson, P.B., Chambers, J.E., Meldrum, P.I., Gunn, D.A., Ogilvy, R.D., Kuras, O., 2010. Predicting the movements of permanently installed electrodes on an active landslide using time-lapse geoelectrical resistivity data only. Geophys. J. Int. 183, 543–556. https://doi.org/10.1111/j.1365-246X.2010.04760.x.
Wistuba, M., Gorczyca, E., Malik, I., Yu, R., Ślęzak, A., 2024. Divergent patterns of landslide activity and triggering factors at a local scale of a single mountain massif (Island Beskid Mts., Western Carpathians, Poland). Eng. Geol. 335, 107531. https://doi.org/10.1016/j.enggeo.2024.107531.
Wood, C.M., Cox, B.R., 2012. A comparison of MASW dispersion uncertainty and bias for impact and harmonic sources. In: GeoCongress 2012: State of the Art and Practice in Geotechnical Engineering. Oakland, CA, USA, pp. 2756–2765. https://doi.org/10.1061/9780784412121.282.
Wróbel, M., Kłeczek, I.S., Marciniak, A., Majdański, M., Kowalczyk, S., Nawrot, A., Cader, J., 2023. Integrated geophysical imaging and remote sensing for enhancing geological interpretation of landslides with uncertainty estimation — a case study from Cisiec, Poland. Remote Sens. 15, 238. https://doi.org/10.3390/rs15010238.
Xia, K., Hilterman, F., Hu, H., 2018. Unsupervised machine learning algorithm for detecting and outlining surface waves on seismic shot gathers. J. Appl. Geophys. 157, 73–86. https://doi.org/10.1016/j.jappgeo.2018.07.003.